Biofabrication

International Society for Biofabrication

PAPER

Femtosecond laser induced densification within cell-laden hydrogels results in cellular alignment

To cite this article: Zheng Xiong *et al* 2019 *Biofabrication* **11** 035005

Biofabrication

PAPER

Femtosecond laser induced densification within cell-laden hydrogels results in cellular alignment

RECEIVED
10 November 2018

REVISED
26 February 2019

ACCEPTED FOR PUBLICATION
13 March 2019

PUBLISHED
5 April 2019

Zheng Xiong, Haiyan Li, Puskal Kunwar, Yin Zhu, Rafael Ramos, Shannon Mcloughlin, Tackla Winston, Zhen Ma and Pranav Soman

Department of Biomedical and Chemical Engineering, Syracuse University, Syracuse, NY, 13244, United States of America

E-mail: psoman@syr.edu

Keywords: femtosecond laser, gelatin methacrylate, densification, cellular alignment, cell encapsulation

Supplementary material for this article is available online

Abstract

The unique capabilities of ultrafast lasers to introduce user-defined microscale modifications within 3D cell-laden hydrogels have been used to investigate fundamental cellular phenomenon such as adhesion, alignment, migration and organization. In this work, we report a new material modification phenomenon coined as 'densification' and its influence on the behavior of encapsulated cells. Femtosecond laser writing technique was used to write densified lines of width 1–5 μm within the bulk of gelatin methacrylate (GelMA) constructs. We found that densified micro-lines within cell-laden GelMA constructs resulted in preferential and localized alignment of encapsulated human endothelial cells. Degree of cellular alignment was characterized as a function of cell-culture time and the spacing between the densified line patterns. This phenomenon was found to be true for several cell lines, including mouse fibroblasts and osteocytes, and mesenchymal stem cells derived from human induced pluripotent cells. This first report of physical densification using fs lasers can be potentially extended for investigating cell behavior within other photosensitive hydrogels.

1. Introduction

Extracellular matrix mimicking hydrogels have been widely used as model 3D culture systems to uncover underlying mechanisms of cell behavior occurring during development and disease [1–3]. In a typical experimental process flow, (i) cells are encapsulated within a biocompatible synthetic, semi-synthetic or natural hydrogel matrix, followed by (ii) biophysical and/or biochemical manipulation of the hydrogel environment in a controlled fashion, followed by (iii) assessment of the cellular responses by conventional microscopy techniques. Although a large number of research tools have been developed to manipulate hydrogel properties, ultrafast laser writing is the one of few methods capable of providing user-defined micro-to-nanoscale manipulation within a cell-laden hydrogel matrix [3–5].

Femtosecond (fs) laser induced multiphoton processing has been used to manipulate material properties within cell-laden hydrogels with minimal collateral damage to surrounding living cells [6–8]. Fs lasers have been used to immobilize growth factors and adhesive peptides and/or create biophysical voids and channels within cell-laden hydrogels to investigate fundamental cell behavior [2, 3, 9–14]. Also, fs laser writing combined with advances in orthogonal chemistry have also allowed the concurrent patterning of stiffness and temporal control over soluble factors to better complex *in vivo* environments. Fs laser based ablation and degradation of unmodified hydrogels and hydrogels modified with photo-cleavable groups respectively have allowed the *in situ* pattering of microchannels in the presence of living cells. This method has been widely used to produce hollow micro-features within a range of hydrogels to spatially direct cell migration, guide multicellular organization to form neural and micro-vasculature networks, and engineer disease models with embedded fluid flows.

Although never reported in cell-laden hydrogels, fs laser writing within glass, polymers, silicone hydrogels, and BSA protein solutions have been reported to cause a change in refractive indices [15–17]. The change in RI, especially in glass and polymers has been

exploited to create optical waveguides, diffraction gratings, and optical storage devices [10, 18, 19]. Although not fully understood, the underlying cause for a change in refractive indices in various materials have been attributed to crosslinking, material densification due to collapse of polymer chains, phase separation or changes in functional groups [20–23]. For the first time, we report that fs lasers can introduce material modification in form of 'densification' within the bulk of 3D cell-laden hydrogel constructs. We also report that all the cell types tested in this work sense the densified patterns and preferential align along micro-patterns, resulting in localized, user-defined and 3D cellular alignment.

2. Materials and methods

2.1. Synthesis of GelMA, LAP photoinitiator, and prepolymer preparation

Gelatin Methacrylate (GelMA) macromer was synthesized using a previously reported protocol [24]. Briefly, 10 g porcine skin gelatin (Sigma Aldrich, St. Louis, MO) was mixed in 200 ml phosphate buffered saline (PBS, Thermo Fisher Scientific), stirred at 45 °C, and methacrylic anhydride was added to the solution and stirred for 3 h. After stirring, the mixture was dialyzed against distilled water for 1 week at 40 °C to remove the unreacted groups from the solution. The dialyzed GelMA was lyophilized in a freeze dryer (Labconco, Kansas City, MO) for one week. Lithium phenyl-2,4,6-trimethylbenzoylphosphinate (LAP) was synthesized in a two-step process according to the literature. At room temperature and under argon, 2,4,6-trimethylbenzoyl chloride (4.5 g, 25 mmol) was added dropwise to continuously stirred dimethyl phenylphosphonite (4.2 g, 25 mmol). The reaction mixture was then stirred for 24 h therefore an excess of lithium bromide (2.4 g, 28 mmol) in 50 ml of 2-butanone was added to the reaction mixture from the previous step which was then heated to 50 °C. After 10 min, a solid precipitate formed. The mixture was then cooled to room temperature, allowed to rest overnight and then filtered. The filtrate was washed with 2-butanone (3 × 25 ml) to remove unreacted lithium bromide and dried under vacuum to give LAP (6.2 g, 22 mmol, 88%) as a white solid. To prepare either 7% or 10% (w/v) GelMA, a stock solution was prepared by mixing 0.7 or 1 g of freeze dried GelMA with 10 ml of deionized water (dissolved at 40 °C), and 0.25% (w/v) UV photoinitiator lithium phenyl-2,4,6-trimethylbenzoylphosphinate (LAP) was added into the solution. GelMA pre-polymer solution was filtered (pore size = 0.2 μm) and used within 2 h after preparation.

2.2. Characterization of mechanical properties of GelMA constructs

In-situ photo-rheometry was performed to observe the changes in the storage modulus (G') during UV exposure of specific duration of UV exposure [24]. A modified standard AR 2000 Rheometer (TA Instruments, New Castle, DE) fitted with a 45 deg reflective mirror and custom-made insert allowing for the attachment of a UV-light collimating tube from a UV lamp (output power 3.5 mW cm^{-2}, OmniCure S2000) [24, 25]. Samples were tested at 25 °C and at 1 Hz under 1% strain using an 8 mm diameter bottom plate and 50 μl of prepolymer solution. Gap distance was set at 250 μm to match the height of the GelMA samples used in this study. Total test time was fixed at 10 min, with the UV light being turned on after 1 min for a specific duration (5–60 s). To measure the elastic modulus of partially crosslinking GelMA samples, the following procedure was used. 50 μl of the GelMA prepolymer solution (7% w/v; 0.25% LAP) was pipetted into custom made PDMS wells (8 mm diameter, 0.25 mm thickness) and exposed to UV light (output power 3.5 mW cm^{-2}, OmniCure S2000) for a range of predefined time (5–60 s). The crosslinked samples were then transferred to the well plates and incubated in ultra-pure DI water and allowed to swell for 24 h. The storage (G') and loss (G'') modulus of the samples were measured at 0.5% strain for a range of 0.1–100 Hz. The linear regions for both moduli recorded between 1 and 10 Hz were used to calculate the shear (G) and Elastic modulus (E). The Poisson's ratio (υ) was assumed to be 0.4 [26, 27]:

$$E = 2G(1 + \upsilon) \text{ where } G = \sqrt{G'^2 + G''^2}. \quad (1)$$

2.3. Cell culture

Human umbilical vein endothelial cells (HUVECs) were maintained in VascuLife Basal Medium (Lifeline Cell Technology) supplemented with VascuLife VEGF LifeFactors Kit (Lifeline Cell Technology), 1% Penicillin/Streptomycin (P/S) on gelatin-coated flasks. Medium of HUVECs were changed every 2 days, and passage 4–9 were used for cell encapsulation studies. Mouse 10T1/2 fibroblasts were maintained in Basal Medium Eagle (BME, Gibco) supplemented with 10% Fetal Bovine Serum (FBS), 1% P/S and 1% Glutamax, and passage numbers below 17 were used for cell encapsulation studies. Mouse IDG-SW3 late osteoblasts were maintained in α-Modified Eagle Medium (α-MEM) supplemented with 10% FBS, 1% P/S, 1% Glutamax and 50 U/ml IFN-γ on rat tail type I collagen-coated flasks, and passage 5–15 were used for cell encapsulation studies. All cell lines in this work, except for mouse IDG-SW3 late osteoblast cell line, were cultured in a cell culture incubator in 5% CO_2 atmosphere at 37 °C. IDG-SW3 late osteoblasts were cultured in 33°C incubator with 5% CO_2. The hiPSCs were maintained on 6-well plates coated with growth factor reduced Geltrex (Life Technologies, Ca# A1413302) in Essential 8 (E8) media (Life Technologies, Ca# A1517001). To start MSC differentiation, hiPSC were maintained in E8 for two additional days,

and then induced for differentiation at 'day 0' with differentiation media that consists of 10 ng ml^{-1} bFGF (R&D Systems Ca# 233-FB), 4 μM SB431542 (Stemgent, Ca# 04–0010–10) and 4 μM WNT agonist CHIR99021 (Stemgent, Ca# 04-2004) in Essential 6 (E6) media (Life Technologies, A1516401). Differentiation media was changed daily for the next 5 d. On day 6, the differentiated cells were plated as MSC Passage 0 (MP0) on a Geltrex coated 6-well plate in a serum-free MSC culture media (CTS StemPro MSC SFM), (Life Technologies, A1033201) for continuous passages. After MP5, the differentiated cells gained the cellular morphology and molecular characteristics of MSCs. For alignment experiment in the GelMA hydrogel, hiPSC-MSCs were maintained in Dulbecco's Modified Eagle Medium (DMEM, Gibco) supplemented with 10% FBS, 1% P/S and 1% Glutamax on attachment factor protein (Gibco)-coated flasks, and passage 10–15 were used for encapsulation.

2.4. Femtosecond laser writing setup

Custom-built fs-laser platform was designed and built by combining a Ti:Sapphire fs laser (Coherent, Chameleon, USA) with a Zeiss Microscope (Observer Z1, Germany) (SI-1 is available online at stacks.iop.org/BF/11/035005/mmedia). In this setup, a 730 nm femtosecond laser beam with a repetition rate of 80 MHz was passed through an isolator that prevented back scattering. A $\lambda/2$ waveplate in combination with a Glan–Taylor polarizer was used to control laser power, measured by a power meter (Newport, USA). Two biconvex lens were used to expand the beam to fill the back aperture of the objective lens. A pinhole was used to filter out diffraction noise at the periphery of the beam. An objective 20 × (Zeiss, Germany) was used to process GelMA samples. A filter (Semrock, USA) was used to block out the UV spectrum of the illumination light source to avoid any crosslinking effects on GelMA samples. This setup was used to introduce patterns in the center or the mid-point of both GelMA and cell-laden GelMA samples. User-defined patterns were designed using AutoCAD and then converted to visual basic code. Line patterns were written at varying speeds and laser powers using a custom written algorithm that controls the stage and laser shutter based on a computer-generated design. Patterns were visualized in real time under bright-field and contrast microscopy. In this work, laser dosage (E) was defined as

$$E = Intensity \times Time, \quad (2)$$

where laser intensity, $I = \frac{P}{\pi R^2}$, exposure time, $T = \frac{2R}{V}$, airy radius of laser beam, $R = \frac{0.61\lambda}{NA}$, P is the average power measured by a power-meter right before the objective, V is the stage scanning speed, λ is the wavelength of fs laser and NA is the numerical aperture of the objective.

2.5. Fs-laser modifications within cell-laden GelMA

Prior to encapsulation, cells (1×10^6 cells ml^{-1}) were trypsinized, counted and mixed with 10% GelMA (w/v) pre-polymer solution and 0.36% LAP photo-initiator, to achieve a final concentration of 7% GelMA with 0.25% LAP. The cell-laden pre-polymer solution (20 μl) was pipetted between glass slide and methacrylated glass coverslip (spacing = 250 μm) (SI-1). UV light was exposed at a power of 3.5 mW cm^{-2} for 5 s to obtain partially crosslinked cell-laden GelMA samples. Femtosecond laser writing system was then used to write user-defined patterns at the center of the GelMA samples. Patterns were written at varying depths of the sample, while keeping the laser power and speed constant. (800 mW, 50 μm s^{-1}). The ability to introduce laser-based modification during ongoing cell culture was demonstrated using IDG-SW3-laden GelMA samples. In this experiment, cell encapsulated was performed on day 0, followed by introduction of densified lines after 24 h. All samples were cultured in 12-well-plates (Fisher Scientific) under standard culture conditions (37 °C, 5% CO_2) using the specific media for each cell type. The media were changed every 2 d.

2.6. Quantification of cellular viability and alignment

Viability of cells were determined using a Live/Dead Assay Kit. Samples were incubated in calcein AM and ethidium homodimer (Invitrogen) at concentration of 0.5 and 2 μl ml^{-1}, and fluorescence microscope (Nikon Eclipse Ti) was used to determine cell viability using ImageJ software. To determine cellular morphology, samples were stained for f-actin and nuclei. At pre-determined time-points, cells were fixed with 4% formaldehyde (Invitrogen, Carlsbad, CA) for 30 min, soaked in 2% Triton X-100 in DPBS for 30 min, and subsequently stained with phalloidin (Alexa-Fluor 568, Invitrogen) (1/100 dilution in DPBS) (45 min at RT) and with 1.25 μg ml^{-1} DAPI (Life Technologies) (5 min at RT) to visualize f-actin and cell nuclei respectively. In another experiment, Cytochalasin D, a known inhibitor of actin dynamics, was added to the media of selected 10T1/2-laden GelMA samples (0.25 μg ml^{-1}) on day 0 or day 3 and these samples were fixed on day 3 and day 6 respectively, before immunostaining them for DAPI and phalloidin. Cell images were taken by inverted microscope (Nikon Eclipse Ti) and quantified using ImageJ software. The cell nuclei orientation was defined as the orientation of the major axis of individual nuclei with respect to the densified line patterns. Nuclei orientation angle less than 10° was identified as completely aligned cells. The nuclear shape index (circularity = 4*π*area/perimeter^2), an indicator of the shape of the cells, was also measured. The shape index of 1 was designated as a perfectly circular cell, while a decrease in the shape index was used to assess cellular elongation.

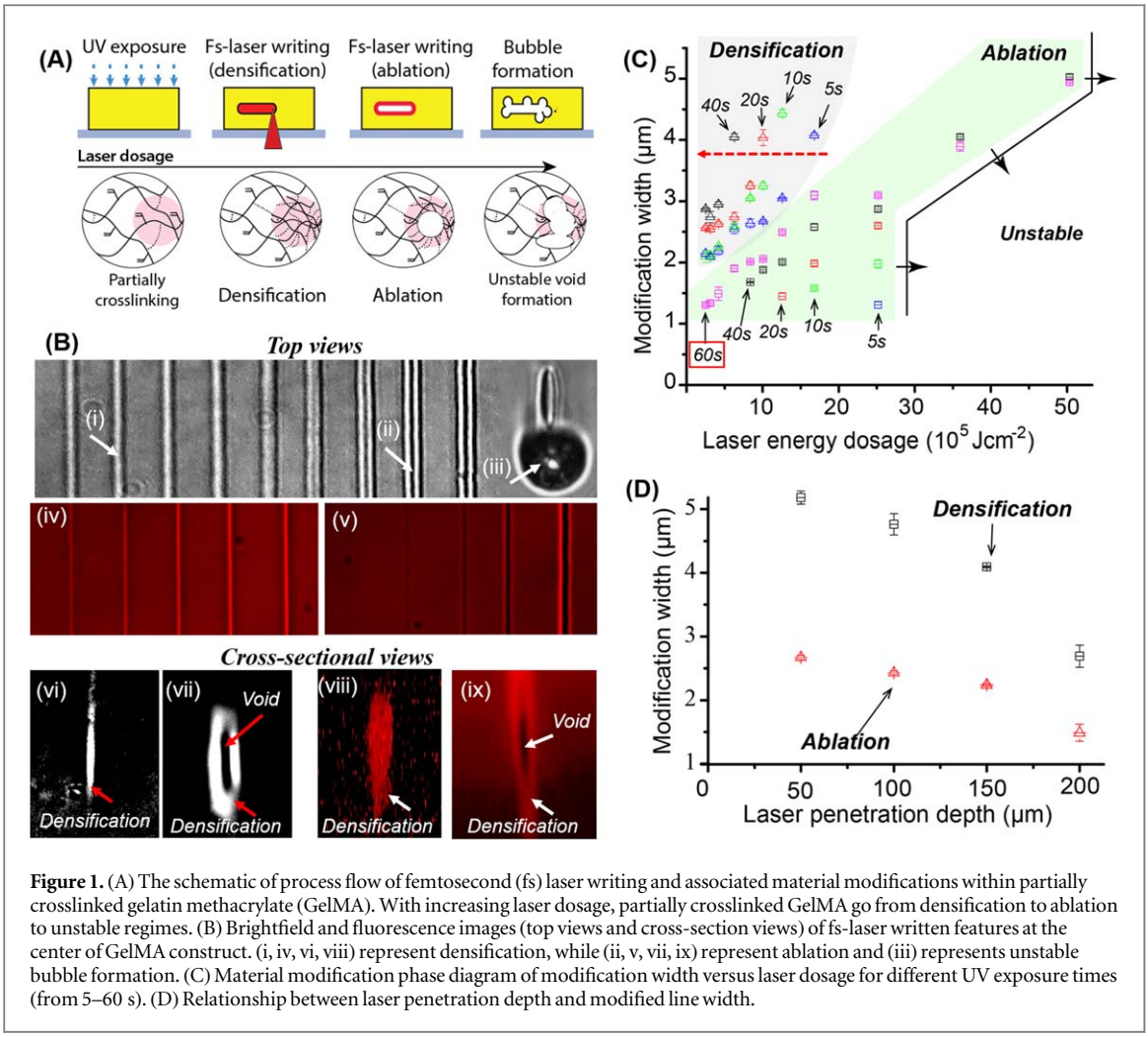

Figure 1. (A) The schematic of process flow of femtosecond (fs) laser writing and associated material modifications within partially crosslinked gelatin methacrylate (GelMA). With increasing laser dosage, partially crosslinked GelMA go from densification to ablation to unstable regimes. (B) Brightfield and fluorescence images (top views and cross-section views) of fs-laser written features at the center of GelMA construct. (i, iv, vi, viii) represent densification, while (ii, v, vii, ix) represent ablation and (iii) represents unstable bubble formation. (C) Material modification phase diagram of modification width versus laser dosage for different UV exposure times (from 5–60 s). (D) Relationship between laser penetration depth and modified line width.

3. Results

3.1. Laser induced material modifications within partially crosslinked GelMA

Fs laser direct writing system was used to introduce material modifications in form of line patterns within partially crosslinked GelMA in a two-step process (figure 1(A), SI-1). In the first step, a liquid prepolymer GelMA solution (7% or 10%), with 0.25% LAP photoinitiator, was pipetted between methacrylated glass coverslip and glass slide, and exposed to UV light (365 nm, 3.5 mW cm^{-2}) for varying amount of UV times to obtain a GelMA samples of thickness 250 μm. Upon UV exposure, GelMA crosslinking begins to occur through the conversion of the methacrylate double bond into covalent bonds, indicated by an increase in storage and elastic modulus (SI-2). In the second step, focused fs-laser was used to introduce line patterns at the center of a 250 μm thick GelMA sample with increasing laser dosage. To increase laser dosage, the scanning speed was varied while maintaining a constant laser intensity. Based on the absorption spectra of GelMA, a wavelength of 730 nm was used to introduce material modifications using two-photon absorption at the fs-laser focus. (SI-3),

During the fs-laser writing experiments, two material modification regimes, densification and ablation, were identified (figure 1). In the densification regime, fs laser writing at lower laser dosage drives two photon crosslinking of partially crosslinking GelMA by conversion of free acrylate groups into covalent double bonds. Further increase in laser dosage likely results in collapse and compaction of GelMA chains resulting in a densified region, that appears brighter as compared to the rest of the GelMA (figure 1(B)) To verify that 'densification' is different from 'crosslinking' of partially-crosslinked GelMA samples, the written lines were irradiated with UV lamp for 30 min to ensure complete crosslinking of GelMA. We found that modified lines written with fs-laser continue to be clearly identified under brightfield imaging and fluorescence imaging using Rhodamine B stained GelMA (figure 1(B)), suggesting that densification of GelMA is not similar to fully-crosslinked GelMA.

Figure 1(C) shows the phase diagram for both densification and ablation processing regimes, with the width of the modified (densified or ablated) line on the *X* axis and increase in the laser energy dosage on the *Y* axis. Within the plot, pink, black, red, green, and blue color symbols represent UV exposure times of 60, 40,

20, 10 and 5 s respectively. Changes in UV exposure times influence the degree of partial crosslinking of GelMA samples before a focused fs laser is irradiated within the samples. In the densification regime, the width of the densified lines increase exponentially with an increase in laser dosage (figure 1(C)). With an increase in UV exposure time from 5 to 40 s, the required laser dosage is decreased for achieving same width of densified lines, indicated by a shifting of the densification curve towards the left (Red dashed arrow in figure 1(C)). This result implies that during the fs laser writing step, the energy is initially utilized to crosslink partially crosslinked GelMA before being used for densification. For samples with higher degree of crosslinking (higher UV exposure times), the 'densification' regime becomes narrower (UV times of 5–40 s). For fully crosslinked samples (UV time of 60 s) (SI-2), densification disappears completely and material modification shift to the ablation regime (Red square in figure 1(C)). This implies that some degree of partial crosslinking is a necessary condition for densification to occur.

In the ablation regime, increase in laser dosage causes an ablation of a void surrounded by a densified shell (figure 1(B)). In this regime, the channel width increase linearly with fs laser dosage (figure 1(C)). For a fully crosslinking sample (UV time-60 s), ablation occurs even at lower laser dosage, while for partially crosslinked samples (40, 20, 10 and 5 s), laser energy is initially utilized for crosslinking and densification processes, before being utilized for the ablation process. This explains the left shift in the ablation curve with an increase in UV time which corresponds to an increase in partial crosslinking of GelMA. Beyond a critical value of fs-laser dosage, bubble formation is observed depicted as 'unstable' (figure 1(C)). Modification widths in both densification and ablation regimes decreases with increasing laser focus depth within the GelMA samples possibly due to scattering losses (figure 1(D)). In summary, an increase in the laser dosage within partially crosslinked GelMA leads to continuous material modifications from fully crosslinking to densification to ablation to unstable bubble formation.

3.2. Influence of fs-laser induced densification on cell behavior

In this work, we choose to investigate the influence of fs-laser induced densification on cell behavior. Densified lines (10 lines per pattern) were introduced within cell-laden GelMA samples, and cellular viability and morphology of encapsulated cells were characterized. Densified line patterns (width ~3 μm; spacing 50 μm) were written at the center of 7% GelMA constructs (UV exposure times of 5 s) containing human endothelial cells (HUVECs). Cell viability of encapsulated HUVECs was assessed using a standard live/dead assay (figure 2(B)). Results demonstrate no significant differences between laser modified and non-modified control samples. We also found little to no cell death directly above and below the written lines, indicating the highly localized influence of the two-photon writing process. To characterize the morphology of encapsulated cells, HUVECs were encapsulated within 7% GelMA constructs at a cell density of 1 M ml^{-1} using a UV exposure time of 5 s, and nuclei alignment was measured using immunostaining and ImageJ analysis.

Briefly, cells whose nuclei orientation lie within 10° of the orientation of the fs-laser densified lines were considered aligned, and the degree of alignment was plotted in form of histograms displaying the relative percentage of aligned cells normalized with the total number of cells. After 24 h of culture, HUVECs near the densified lines start to spread. By day 3, they align along the direction of the densified lines, and the degree of alignment increases by day 5 (figure 2(C)). Results show that for 50 μm line spacing, percentage of cell alignment increase from 28.89 $\pm$ 2% on day 1, to 41.74 $\pm$ 3.65% on day 3, to 57.02 $\pm$ 5.51% on day 5 respectively as compared to un-patterned control (10.56 $\pm$ 1.63%) (figure 2(D)). Similar trend of an increase in nuclei alignment as a function of culture time can also be observed for 100 μm and 200 μm line spacing (data not shown). Nuclear shape index, that assumes values between 1 for ideal circular shape and decreasing values for elongated morphology, decreased as a function of culture time (figure 2(E)). The spacing between densified lines also influenced the degree of cell alignment. For day 5, as line spacing increases from 50 to 200 μm, the cell alignment drops from 57.02 $\pm$ 5.51% to 31.92 $\pm$ 3.79%, although even with 200 μm spacing, cell alignment is still significantly higher than control group (figure 3(B)). Nuclear shape index also decreased with increased line spacing (figure 3(C)). To investigate whether f-actin is involved in preferential cell alignment along densified lines, cytochalasin D (CytoD), a widely used inhibitor of actin dynamics, was introduced into the culture system at day 3 and day 6. Results show that cell alignment is inhibited in both cases as compared to control patterned group (SI-4). More work needs to be undertaken to elucidate the underlying mechanism related to localized nuclei elongation, and its influence on overall cell function.

3.3. Design flexibility of densification induced cell alignment method

3.3.1. Densification induced cell-alignment across cell types

To test whether densification induced cellular alignment can be extended to other cell types, cell-laden GelMA samples were prepared using mouse 10T1/2 s fibroblasts, mouse IDG-SW3 osteocytes, and human induced pluripotent stem cells-derived mesenchymal

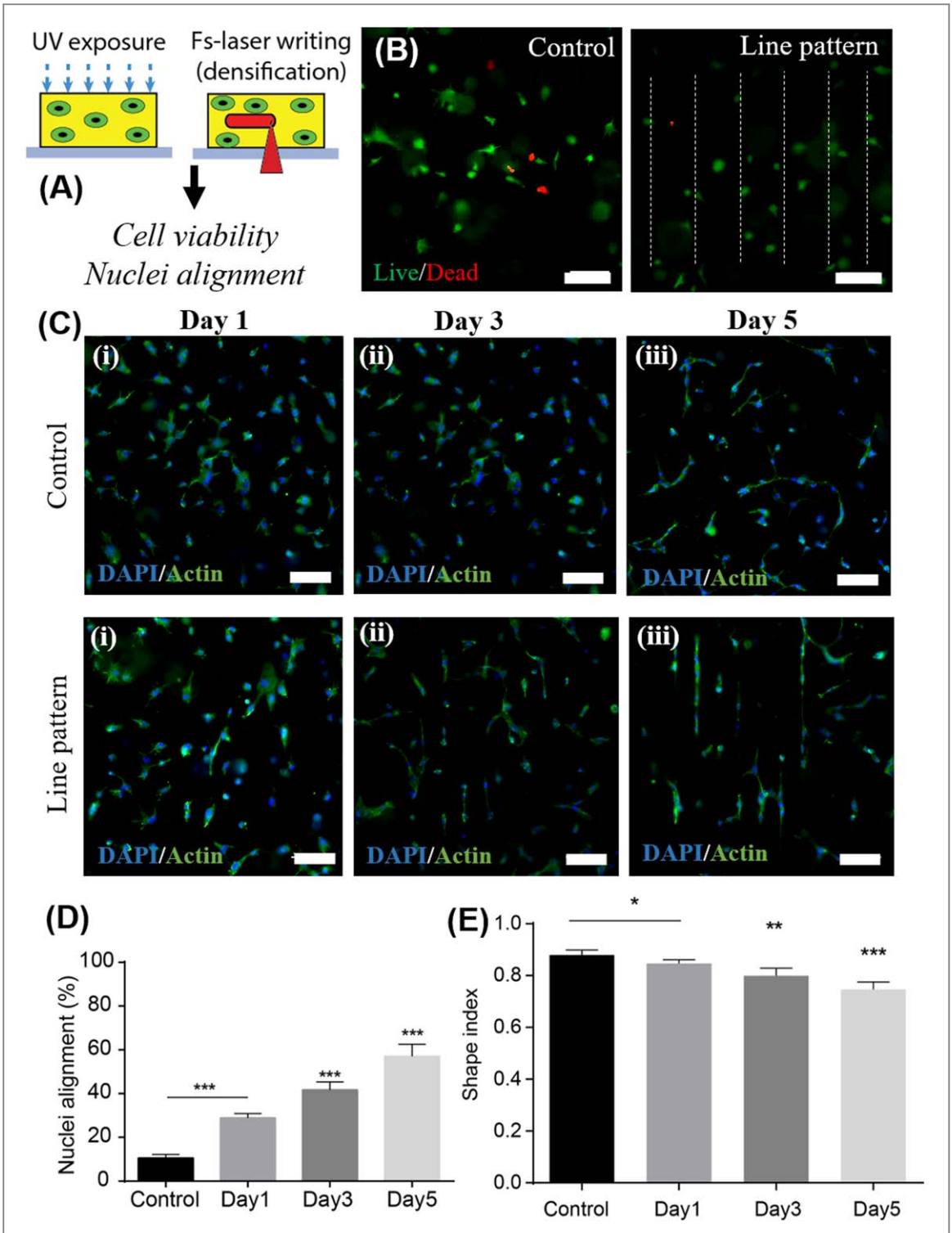

Figure 2. (A) Schematic of experimental design; cell-laden GelMA was partially crosslinked using a UV exposure time of 5 s, followed by fs laser writing of densified line patterns at the center of the samples. (B) Characterization of cell viability 24 h after fabrication using a live (green)-dead (red) assay. (Line spacing-50 μm, dashed white lines) (C) Fluorescence images showing nuclei (blue) and actin (green) morphology of HUVECs around un-patterned and patterned regions on (i) Day 1, (ii) Day 3 and (iii) Day 5. (D) Plot of nuclear alignment versus days in culture for patterned regions for a line spacing of 50 μm. (D) Plot of nuclear shape index versus days in culture for patterned regions for line spacing of 50 μm. (Scale bar: 100 μm) (Error bars: Mean $\pm$ SD; $^{***}p < 0.001$; $^{**}p < 0.01$; $^{*}p < 0.05$) controls shows un-patterned results on Day 5.

stem cells (hiPSC-MSCs). Similar to what we observed with HUVECs, results show that patterned regions show significantly higher percentage of cellular alignment for IDG-SW3 ($41.47 \pm 7.79\%$; $p < 0.001$), 10T1/2 s ($39.07 \pm 1.96\%$; $p < 0.001$), and hiPSCs-MSCs ($30.45 \pm 5.94\%$; $p < 0.01$), as compared to the un-patterned regions (figure 4). A corresponding decrease in the mean nuclear shape index was also measured, which demonstrates a significant increase in cellular elongation along the patterned regions.

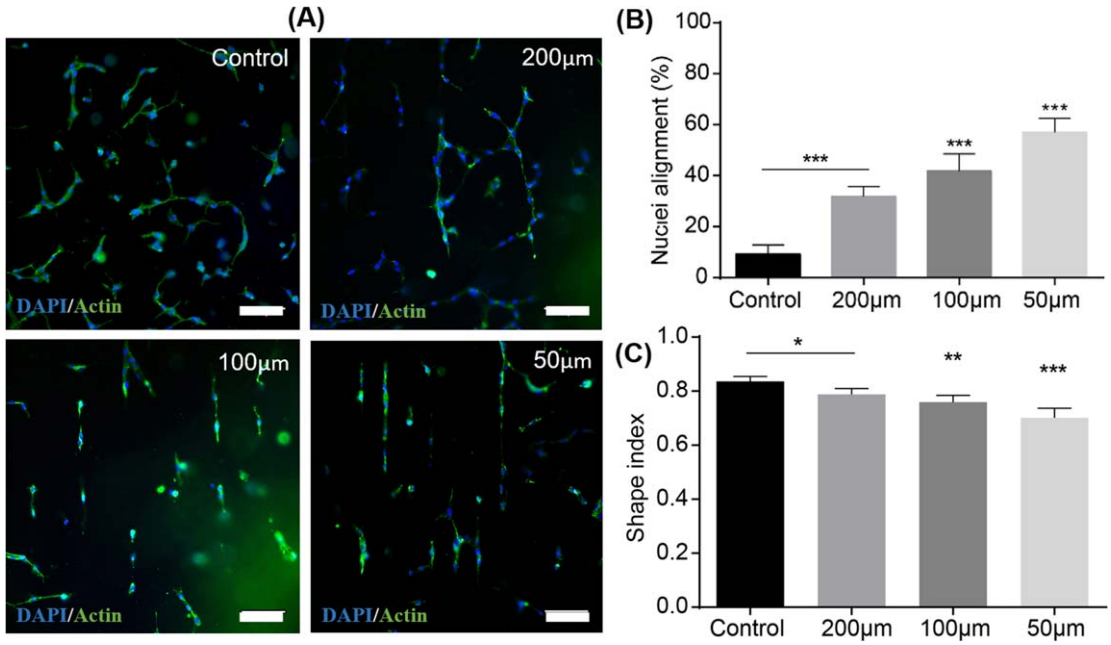

Figure 3. (A) Fluorescence images showing nuclei (blue) morphology and actin (green) morphology of HUVECs around patterned regions for a lined spacing of 50, 100 and 200 μm on Day 5. Controls shows un-patterned results on Day 5 (B) Quantification of changes in nuclear alignment as a function of line spacing on Day 5. (C) Quantification of changes in shape index as a function of line spacing on Day 5. (Scale bar: 100 μm) (Error bars: Mean $\pm$ SD; $^{***}p < 0.001$; $^{**}p < 0.01$; $^{*}p < 0.05$).

3.3.2. Temporal flexibility of in situ densification

To demonstrate that densified lines can be introduced at any point during an active cell culture experiment, IDG-SW3-laden GelMA was prepared on Day 0, and densified line patterns were introduced on Day 1. Results show an increase in cellular alignment on day 5, demonstrating the temporal flexibility of this method to introduce physical guidance cues during active cell culture. (Dashed box in figure 4).

3.3.3. Densification to align cells along user-defined directions

To demonstrate that laser-induced densification can be used to align encapsulated cells in any user-defined arbitrary alignment configurations, two experiments were conducted. The first experiment introduced two sets of densified lines (spacing-50 μm) with 0° and 90° orientations adjacent to each other within a 10T1/2-laden GelMA (figures 5(A), (B)). Direct written densified lines in 0° and 90° patterns do not overlap and they both are in the same plane at the center of the GelMA sample. Results showed significantly higher cellular alignment along 0° (37.61 $\pm$ 1.62%) and 90° (37.72 $\pm$ 2.04%) as compared to cell alignment in un-patterned regions (10.31 $\pm$ 2.81%). Nuclear shape index demonstrated an increase in cellular elongation along 0° and 90° orientations compared with un-patterned controls. The second experiment introduced densification in the form of a concentric circle pattern within 10T1/2-laden GelMA. Cells align remarkably well to the densified pattern, demonstrating that laser-induced densification can be used to align cells along any arbitrary paths (figure 5(C)). SI-5 shows other complicated patterns that can be generated using this technique.

3.3.4. Influence of out-of-plane densification on cell alignment

To assess the zone of influence of densified structure in the *z*-direction, images were taken at different z-planes above and below the focal plane of the densified line patterns for cell-laden samples. We observed that densification of GelMA can only influence cell alignment in a *z*-range of about 60 μm ($\pm$30 μm on either side) (figure 6(A)). We also observe higher cell spreading in layers closer to the top surface (surface closer to the nutrients), possibly explained by differences in nutrient diffusional limitations at varying depths. To evaluate how sample thickness influences the spreading and alignment of cells, densified line patterns were written at a depth of 80 and 160 μm with a line spacing of 50 μm. After 21 days of culture, cells within layer 1, closer to the surface, showed significant spreading as compared to cells in the vicinity of layer 2. Although the overall cellular alignment in layer 2 is much lower than layer 1 (figure 4(B)), cells that are physically closer to the densified lines are elongated with close to 100% nuclear alignment. Encapsulated cells between layer 1 and 2 (depth range of 100–140 μm) do not show any influence of either densified layers, confirming localized influence even in multilayer pattern.

3.3.5. Influence of GelMA stiffness on densification induced cell alignment

To assess the influence of global stiffness on cell alignment, we compared cell alignment results from

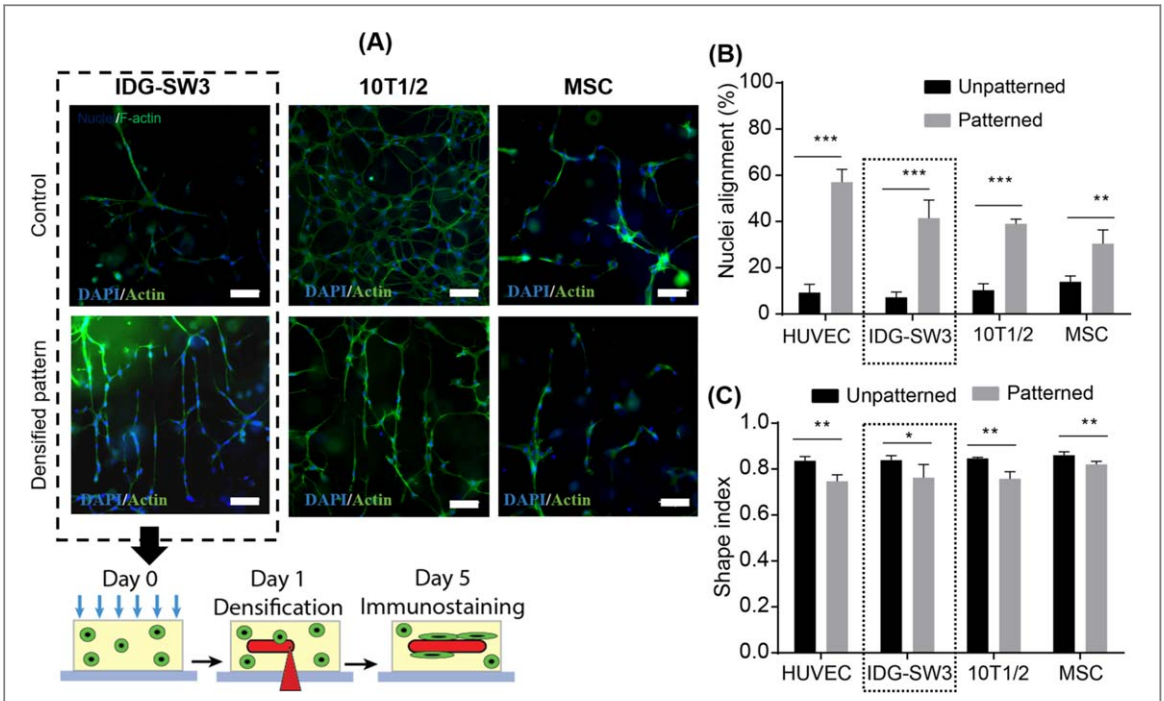

Figure 4. (A) Fluorescence images showing morphology of mouse IDG-SW3 osteoblasts, mouse C3H-10T1/2 fibroblasts, and hiPSCs-MSCs around un-patterned (control) and patterned regions on Day 5. (B) Characterization of changes in nuclear alignment between un-patterned and patterned regions for all cell types (line spacing = 50 μm; Day 5). Dashed square: IDG-SW3 were encapsulated on Day 0, cultured for 24 h, before introducing densified line patterns on Day 1, and immunostaining was performed on Day 5. For all other cells, densified lines were written on Day 0, and immunostaining was performed on Day 5. (C) Plot of nuclear shape index of different cell types for a pattern spacing of 50 μm. (Scale bar: 100 μm) (Error bars: Mean $\pm$ SD; $^{***}p < 0.001$; $^{**}p < 0.01$; $^{*}p < 0.05$).

7% GelMA (3.179 $\pm$ 1.819 kPa) and 10% GelMA (12.198 $\pm$ 2.296 kPa) irradiated with the same UV exposure time of 30 s. (SI-6) The higher global modulus of GelMA resulted in almost 100% degree of nuclei alignment for encapsulated 10T1/2 s close to the densified line patterns (zone 2). Cells even 20 μm away from the densified lines showed no nuclei alignment (zone 1) (figure 7). The overall cell spreading of 10% GelMA (30 s) is limited as compared to both 7% GelMA (30 s from SI-6, and 5 s from figure 4(A)). Thus, it is clear that global stiffness of GelMA prior to fs-laser densification also influences the cellular response.

4. Discussion

Femtosecond (fs) laser is capable of introducing internal modifications within transparent materials due to their unique nonlinear two-photon absorption property. In this work, we report material modification in form of densification within GelMA. Previously, fs laser writing has shown the densification phenomenon within glass, polymers, silicone hydrogels and BSA protein solutions, however the underlying mechanisms are not well understood. In silica glass, PMMA polymer and silicone hydrogels, densification was linked to a change in their refractive index property [16, 21]. In these studies, the changes in refractive indices were attributed to the generation of shockwaves [28], the formation of color centers [29], and structural material modifications [16]. In another study with BSA proteins, densification was shown to induce volume contraction and changes in topography. [30] Similar to previous reports, we hypothesize that thermal accumulation induced by high repetition rate pulsed laser (80 MHz) could result in localized additional crosslinking within GelMA that expels water in the laser focus, resulting in possible collapse and entanglement of chains or material densification that can be visualized by a change in refractive index [31]. In the ablation regime, we observe a void surrounded by a densified shell within GelMA hydrogel. This result also aligns well with similar studies with glass, silica and some thermoplastics that have demonstrated the presence of shockwaves and densified shell formation around voids [32]. Brightfield images clearly show the presence of a dark center line surrounded by a bright region and adjoining darker regions (figure 1(B)) that point to the creation of compaction and rarefaction waves during laser writing process.

Although, fs laser enabled material modifications of hydrogels have been used to investigate cellular adhesion, migration, alignment and differentiation, we report the influence of densification within cell-laden GelMA. We found that fs laser induced densification material modification within cell-laden GelMA is able to provide preferential localized control over cellular alignment within GelMA, a widely used

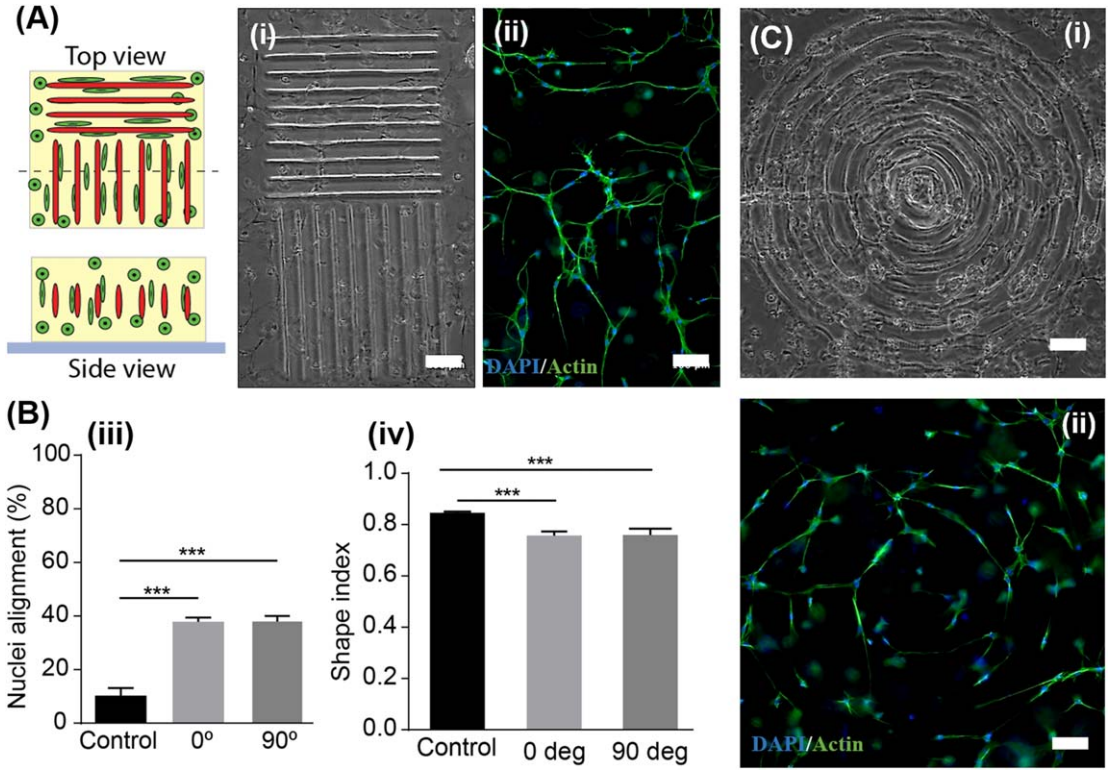

Figure 5. (A) Schematic of the 0° and 90° line pattern design and representative brightfield (i) and fluorescence images (ii) showing alignment of 10T1/2 cells in the vicinity of patterns (line spacing=50 μm; Day 5). (B) Plots of (i) nuclear alignment and (ii) nuclear shape index for cells in the vicinity of patterns within 10T1/2-laden GelMA as compared to cells from the un-patterned regions. (C) Representative brightfield (i) and fluorescence image (ii) showing cellular alignment around user-defined concentric-circle patterns (spacing=50 μm; Day 5) within 10T1/2-laden GelMA. (Scale bar: 100 μm) (Error bars: Mean $\pm$ SD; $^{***}p < 0.001$; $^{**}p < 0.01$; $^{*}p < 0.05$).

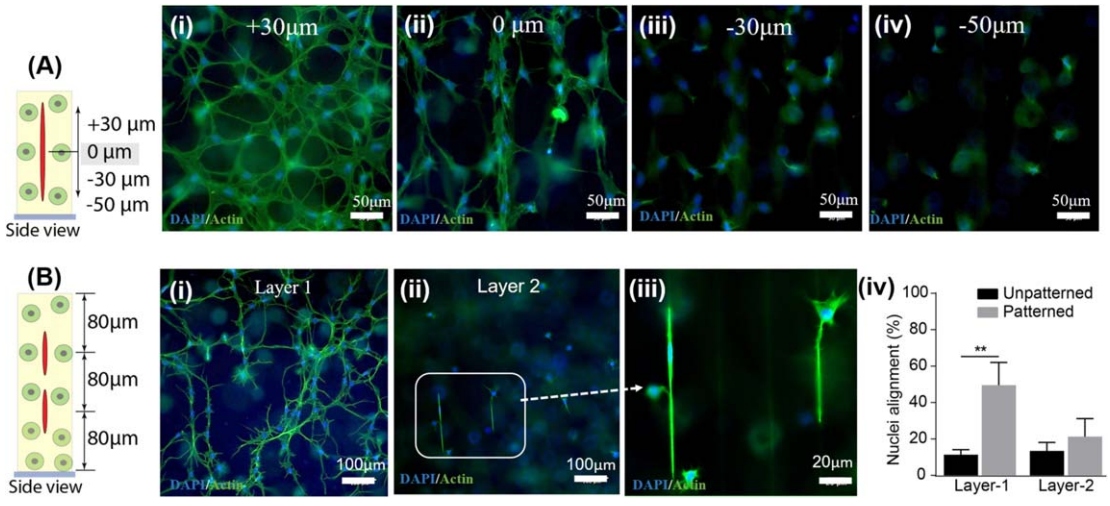

Figure 6. (A) Schematic and representative fluorescence images captured at different z-planes within 10T1/2-laden GelMA. (B) Schematic of a line patterns written in two distinct layers. Fluorescence images from (i) layer 1 (80 μm from the top surface), and (ii, iii) layer 2 (160 μm from the top surface). (iv) Plot shows differences in nuclei alignment between layers 1 and 2 from un-patterned and patterned regions. (Error bars: Mean $\pm$ SD; $^{***}p < 0.001$; $^{**}p < 0.01$)

naturally derived hydrogel. This is a new method to align cells in arbitrary patterns within cell-laden hydrogels. Previously, inspired by the native extracellular matrix, significant research has been directed towards controlling the spatial alignment and organization of cells [33–36]. Although 2D micro/nano-patterns are widely used to align cells, controlling the organization of cells within a 3D hydrogels remains a challenge [35, 37]. Large scale or global alignment of cells within gels have been achieved via (i) partially constrained with matrigel or collagen gels [38, 39], (ii) use of external stimuli such as mechanical stretch

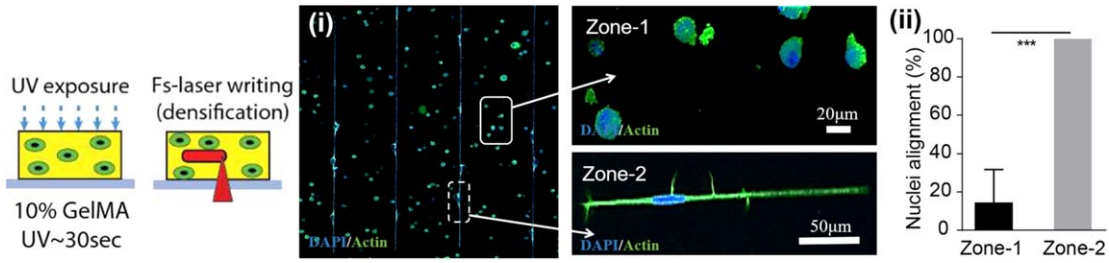

Figure 7. Confocal image taken at center of patterned region within 10T1/2-laden GelMA (10% GelMA, UV crosslinking time- 30 s). Cells do not demonstrate alignment in regions between densified line patterns (zone 1), while cells demonstrate 100% degree of alignment in the vicinity of densified lines (zone 2).

[40], electrical impulse [41] and flow induced shear stress [42], or (iii) micropatterning using PDMS-mold with parallel grooves [37, 43]. All these methods involve complicated processing steps and do not provide local and/or user-defined control over cellular alignment. Two photon laser processing have also been used to pattern cell adhesive ligands within 3D gels to direct cellular migration and alignment [7], however this method requires specialized hydrogels, and are limited by low hydrogel-adhesive ligand conjugation efficiency. The densification approach does not require specialized chemical modification (photolabile groups) [3, 13], inclusion of nanoparticle for enabling two-photon induced thermal degradation of micro-channels within hydrogels [12], or any external stimulation or guidance systems. The fs-laser enabled densification method allows the introduction of patterns during active cell culture providing temporal design flexibility. This novel method could be used to investigate cell behavior within 3D hydrogel systems. For instance, fs-laser densification can be potentially used as a new tool to recreate localized variations in stiffness of 3D extracellular matrix by fs-laser densification. This will be important in elucidating new mechanisms of metastasis, as well as migratory behaviors during wound healing and development that have been shown to be influenced by spatial and localized variations in matrix stiffness [44–46].

5. Conclusion

In this work, we report a new material modification phenomenon coined as 'fs-laser induced densification' within widely used GelMA hydrogels. It was found that introduction of densified line-patterns within cell-laden GelMA resulted in preferential and localized cellular alignment. This method is capable of aligning variety of encapsulated cells in user-defined patterns. We show that densified patterns can be introduced during ongoing cell culture experiments. This first report of physical densification within cell-laden GelMA can be potentially extended to study cell behavior within a range of other photosensitive hydrogels.

Acknowledgments

PS acknowledge support from the National Science Foundation (NSF) (CMMI-1634997). ZM acknowledge the support from Nappi Family Foundation Research Scholar Project.

Author contribution

ZX and HL contribute equally to this work. ZX and PS conceived the idea, designed the experiments, and took a leading role in writing the manuscript; RR and SM performed the material characterization; ZX, PK and YZ performed laser writing experiments and associated analysis; HL performed cell studies and analysis of cellular alignment; TW and ZM differentiated and provided the mesenchymal stem cells from human induced pluripotent stem cells. ZM provided help with fluorescence microscopy.

ORCID iDs

Tackla Winston https://orcid.org/0000-0002-7419-5141
Pranav Soman https://orcid.org/0000-0001-9456-0030

References

[1] Edmondson R, Broglie J J, Adcock A F and Yang L 2014 Three-dimensional cell culture systems and their applications in drug discovery and cell-based biosensors *Assay Drug Dev. Technol.* **12** 207–18
[2] Tam R Y, Smith L J and Shoichet M S 2017 Engineering cellular microenvironments with photo-and enzymatically responsive hydrogels: toward biomimetic 3D cell culture models *Acc. Chem. Res.* **50** 703–13
[3] Pradhan S, Keller K A, Sperduto J L and Slater J H 2017 Fundamentals of laser-based hydrogel degradation and applications in cell and tissue engineering *Adv. Healthcare Mater.* **6** 1700681
[4] Ovsianikov A, Mironov V, Stampfl J and Liska R 2012 Engineering 3D cell-culture matrices: multiphoton processing technologies for biological and tissue engineering applications *Expert Rev. Med. Devices* **9** 613–33
[5] Thiele J, Ma Y, Bruekers S M C, Ma S and Huck W T S 2014 25th anniversary article: designer hydrogels for cell cultures: a materials selection guide *Adv. Mater.* **26** 125–48

[6] Sima F, Sugioka K, Vázquez R M, Osellame R, Kelemen L and Ormos P 2018 Three-dimensional femtosecond laser processing for lab-on-a-chip applications *Nanophotonics* **7** 613–34

[7] Lee S-H, Moon J J and West J L 2008 Three-dimensional micropatterning of bioactive hydrogels via two-photon laser scanning photolithography for guided 3D cell migration *Biomaterials* **29** 2962–8

[8] Vogel A, Noack J, Hüttman G and Paltauf G 2005 Mechanisms of femtosecond laser nanosurgery of cells and tissues *Appl. Phys.* B **81** 1015–47

[9] Culver J C, Hoffmann J C, Poché R A, Slater J H, West J L and Dickinson M E 2012 Three-dimensional biomimetic patterning in hydrogels to guide cellular organization *Adv. Mater.* **24** 2344–8

[10] Gattass R R and Mazur E 2008 Femtosecond laser micromachining in transparent materials *Nat. Photon.* **2** 219

[11] Seliktar D 2012 Designing cell-compatible hydrogels for biomedical applications *Science* **336** 1124–8

[12] Hribar K C, Meggs K, Liu J, Zhu W, Qu X and Chen S 2015 Three-dimensional direct cell patterning in collagen hydrogels with near-infrared femtosecond laser *Sci. Rep.* **5** 17203

[13] Tibbitt M W, Kloxin A M, Dyamenahalli K U and Anseth K S 2010 Controlled two-photon photodegradation of PEG hydrogels to study and manipulate subcellular interactions on soft materials *Soft Matter* **6** 5100–8

[14] Brandenberg N and Lutolf M P 2016 *In situ* patterning of microfluidic networks in 3D cell-laden hydrogels *Adv. Mater.* **28** 7450–6

[15] Gandara-Montano G A, Stoy V, Dudič M, Petrák V, Haškovcová K and Knox W H 2017 Large optical phase shifts in hydrogels written with femtosecond laser pulses: elucidating the role of localized water concentration changes *Opt. Mater. Express* **7** 3162–80

[16] Chan J W, Huser T, Risbud S and Krol D M 2001 Structural changes in fused silica after exposure to focused femtosecond laser pulses *Opt. Lett.* **26** 1726–8

[17] Kaehr B and Scrymgeour D A 2016 Direct-write graded index materials realized in protein hydrogels *Appl. Phys. Lett.* **109** 123701

[18] Ding L, Blackwell R I, Künzler J F and Knox W H 2008 Femtosecond laser micromachining of waveguides in silicone-based hydrogel polymers *Appl. Opt.* **47** 3100–8

[19] Ramirez L P R, Heinrich M, Richter S, Dreisow F, Keil R, Korovin A V, Peschel U, Nolte S and Tünnermann A 2010 Tuning the structural properties of femtosecond-laser-induced nanogratings *Appl. Phys.* A **100** 1–6

[20] Bille J F, Engelhardt J, Volpp H-R, Laghouissa A, Motzkus M, Jiang Z and Sahler R 2017 Chemical basis for alteration of an intraocular lens using a femtosecond laser *Biomed. Opt. Express* **8** 1390–404

[21] Wochnowski C, Eldin M A S and Metev S 2005 UV-laser-assisted degradation of poly (methyl methacrylate) *Polym. Degrad. Stab.* **89** 252–64

[22] Träger J, Heinzer J, Kim H C and Hampp N 2008 Polymers for *in vivo* tuning of refractive properties in intraocular lenses *Macromol. Biosci.* **8** 177–83

[23] Takeshima N, Narita Y, Tanaka S, Kuroiwa Y and Hirao K 2005 Fabrication of high-efficiency diffraction gratings in glass *Opt. Lett.* **30** 352–4

[24] Chen Y X, Yang S, Yan J, Hsieh M-H, Weng L, Ouderkirk J L, Krendel M and Soman P 2015 A novel suspended hydrogel membrane platform for cell culture *J. Nanotechnol. Eng. Med.* **6** 021002

[25] Chen Y X, Cain B and Soman P 2017 Gelatin methacrylate-alginate hydrogel with tunable viscoelastic properties *Aims Mater. Sci.* **4** 363–9

[26] Qin X H, Wang X, Rottmar M, Nelson B J and Maniura-Weber K 2018 Near-infrared light-sensitive polyvinyl alcohol hydrogel photoresist for spatiotemporal control of cell-Instructive 3D microenvironments *Adv. Mater* **30** 1705564

[27] Kuijpers A J, Engbers G H M, Feijen J, De Smedt S C, Meyvis T K L, Demeester J, Krijgsveld J, Zaat S A J and Dankert J 1999 Characterization of the network structure of carbodiimide cross-linked gelatin gels *Macromolecules* **32** 3325–33

[28] Schaffer C B, Brodeur A and Mazur E 2001 Laser-induced breakdown and damage in bulk transparent materials induced by tightly focused femtosecond laser pulses *Meas. Sci. Technol.* **12** 1784

[29] Hirao K and Miura K 1998 Writing waveguides and gratings in silica and related materials by a femtosecond laser *J. Non-Cryst. Solids* **239** 91–5

[30] Hernandez D S, Ritschdorff E T, Connell J L and Shear J B 2018 *In situ* imprinting of topographic landscapes at the cell–substrate interface *J. Am. Chem. Soc.* **140** 14064–8

[31] Morikawa J, Orie A, Hashimoto T and Juodkazis S 2010 Thermal diffusivity in femtosecond-laser-structured micro-volumes of polymers *Appl. Phys.* A **98** 551–6

[32] Zheng C, Chen T, Hu A, Liu S and Li J Fabrication of 3D embedded hollow structures inside polymer dielectric PMMA with femtosecond laser *Int. Soc. Opt. Photonics* **10018** 1001804

[33] Nikkhah M, Edalat F, Manoucheri S and Khademhosseini A 2012 Engineering microscale topographies to control the cell–substrate interface *Biomaterials* **33** 5230–46

[34] Jeon H, Simon C G and Kim G 2014 A mini-review: cell response to microscale, nanoscale, and hierarchical patterning of surface structure *J. Biomed. Mater. Res.* B **102** 1580–94

[35] Li Y, Huang G, Zhang X, Wang L, Du Y, Lu T J and Xu F 2014 Engineering cell alignment *in vitro Biotechnol. Adv.* **32** 347–65

[36] Hoffman B D, Grashoff C and Schwartz M A 2011 Dynamic molecular processes mediate cellular mechanotransduction *Nature* **475** 316

[37] Aubin H, Nichol J W, Hutson C B, Bae H, Sieminski A L, Cropek D M, Akhyari P and Khademhosseini A 2010 Directed 3D cell alignment and elongation in microengineered hydrogels *Biomaterials* **31** 6941–51

[38] Vader D, Kabla A, Weitz D and Mahadevan L 2009 Strain-induced alignment in collagen gels *PLoS One* **4** e5902

[39] Jang J M, Tran S-H-T, Na S C and Jeon N L 2015 Engineering controllable architecture in matrigel for 3D cell alignment *ACS Appl. Mater. Interfaces* **7** 2183–8

[40] Subramony S D, Dargis B R, Castillo M, Azeloglu E U, Tracey M S, Su A and Lu H H 2013 The guidance of stem cell differentiation by substrate alignment and mechanical stimulation *Biomaterials* **34** 1942–53

[41] Stoppel W L, Kaplan D L and Black Iii L D 2016 Electrical and mechanical stimulation of cardiac cells and tissue constructs *Adv. Drug. Deliv. Rev.* **96** 135–55

[42] Rangarajan S, Madden L and Bursac N 2014 Use of flow, electrical, and mechanical stimulation to promote engineering of striated muscles *Ann. Biomed. Eng.* **42** 1391–405

[43] Norman J J and Desai T A 2005 Control of cellular organization in three dimensions using a microfabricated polydimethylsiloxane–collagen composite tissue scaffold *Tissue Eng.* **11** 378–86

[44] Cox T R and Erler J T 2011 Remodeling and homeostasis of the extracellular matrix: implications for fibrotic diseases and cancer *Dis. Models Mech.* **4** 165–78

[45] Kumar S and Weaver V M 2009 Mechanics, malignancy, and metastasis: the force journey of a tumor cell *Cancer Metastasis Rev.* **28** 113–27

[46] Friedl P and Alexander S 2011 Cancer invasion and the microenvironment: plasticity and reciprocity *Cell* **147** 992–1009